Nanoscale Res Lett (2010) 5:1468–1473
DOI 10.1007/s11671-010-9663-5

NANO EXPRESS

Highly Sensitive Fluorescence Probe Based on Functional SBA-15 for Selective Detection of Hg^{2+}

Xiaoyu Wang · Pan Wang · Zihao Dong · Zhengping Dong · Zongyan Ma · Jian Jiang · Rong Li · Jiantai Ma

Received: 24 March 2010 / Accepted: 3 June 2010 / Published online: 17 June 2010

Abstract An inorganic–organic hybrid fluorescence chemosensor (DA/SBA-15) was prepared by covalent immobilization of a dansylamide derivative into the channels of mesoporous silica material SBA-15 via (3-aminopropyl) triethoxysilane (APTES) groups. The primary hexagonally ordered mesoporous structure of SBA-15 was preserved after the grafting procedure. Fluorescence characterization shows that the obtained inorganic–organic hybrid composite is highly selective and sensitive to Hg^{2+} detection, suggesting the possibility for real-time qualitative or quantitative detection of Hg^{2+} and the convenience for potential application in toxicology and environmental science.

Keywords SBA-15 · Dansylamide · DA/SBA-15 · Hg^{2+} ion · Detection

Introduction

There has been growing interest during the last decade in the development of fluorescent molecular sensors for detecting metal ions in solution [1–5]. This is mainly due to the potential application in biochemistry and environmental monitoring. Fluorescent chemosensors for selective detection of transition metal ions, especially Hg^{2+} ion has also been actively investigated [6–9]. Because Hg^{2+} is the most toxic heavy metal ion with a distinct toxicological profile, and arises from a variety of natural and human-generated sources [10–12], this common pollutant poses severe risks for human health and natural ecosystems. However, many of these systems displayed short-comings in practical use, such as the lack of aqueous solubility, cross-sensitivities toward other metal ions and weak fluorescence intensity. As a result, developing new and practical sensor systems for Hg^{2+} is still a challenge. SBA-15 has generated a great deal of interest in the area of sensors due to its high surface areas and large ordered pores ranging from 2 to 50 nm with narrow size distributions [13–16]. With their use in the preparation of inorganic–organic hybrids for molecular recognition, the high surface area allows the doping of them with a high concentration of sensitive probes, and the highly uniform porosity allows for facile diffusion making them excellent hosts for sensing molecules or ions [17]. For this purpose, a variety of bulky organic functional molecules such as tetraazacyclotetradecane, izocyanurate, and Schiff-base were grafted or incorporated inside the channel of mesoporous materials [18–20]. The design and synthesis of these innovative hybrid mesoporous materials for heavy metal ions detection are of considerable interest and opens up an extraordinary field of investigation. Moreover, using SBA-15 as a solid binding unit has inherent advantages such as optical transparency in the visible region and favorable biocompatibility. This enables such silica-based materials to be promising sensor substrates [21–23]. On the other hand, dansyl group is one of the most attractive fluorophores [24, 25] due to its strong fluorescence, relatively long emission wavelength and easy derivation. Bearing this in mind, we report a new inorganic–organic hybrid fluorescence chemosensor (DA/SBA-15) for Hg^{2+}. Strong signal output in neutral aqueous environments of recognition, high

X. Wang · P. Wang · Z. Dong · Z. Dong · Z. Ma · J. Jiang · R. Li · J. Ma (✉)
College of Chemistry and Chemical Engineering, Lanzhou University, 730000 Lanzhou, People's Republic of China
e-mail: majiantai@lzu.edu.cn

R. Li
e-mail: liyirong@lzu.edu.cn

selectivity, and sensitivity made DA/SBA-15 a potential powerful candidate as a practical fluorescent sensor for Hg^{2+}.

Experimental

Reagents and Chemicals

Tri-block copolymer P_{123} ($EO_{20}PO_{70}EO_{20}$, EO = ethylene oxide, PO = propylene oxide, 5800) was obtained from Aldrich. TEOS ($Si(OCH_2CH_4)_4$) was purchased from.

Sinopharm chemical Reagent Co. Ltd. Dansyl chloride (DC), (3-Aminopropyl)triethoxysilane (APTES) and Perchloric acid salts of various metals were purchased from Alfa Aesar Co. Ltd. All the chemicals were used as received.

Synthesis of SBA-15

SBA-15 was synthesized as reported by Zhao et al. [26]. In a typical synthesis, 2 g P123 was dissolved in 75 ml 2 M HCl solution with stirring, followed by addition of 4 mL TEOS to the homogeneous solution (staring mole ratio: TEOS/P123/HCl/H_2O = 1/0.019/8.4/233). This gel was stirred at 313 K for 24 h and then crystallized at 373 K for 24 h under static condition. The resulting solid was filtered, washed, dried overnight at 373 K and calcined at 823 K in air for 6 h. Thus, SBA-15 was obtained.

Preparation of DA/SBA-15 Composites

3-(Dansylamido)-propyl-triethoxysilane (DA-APTES): a solution of dansyl chloride (0.45 g, 1.65 mmol) in CH_2Cl_2 (10 mL) was added to a solution of (3-aminopropyl)triethoxysilane (APTES, 0.40 mL, 1.7 mmol) and triethylamine (0.30 mL, 2.15 mmol) in the same solvent (10 mL). The mixture was stirred at room temperature for 2 h while monitoring the reaction by TLC (toluene/ethyl acetate 1/1). The solvent was evaporated under reduced pressure, and the crude product was purified by flash chromatography (silica gel, toluene/ethyl acetate 1/1) to afford 0.69 g (92%) of DA-APTES as yellow-bright green oil [27]. ^{1}HNMR: (400 MHz, $CDCl_3$, 25°C): δ (ppm) 0.47(*t*, J = 8.04 Hz, 2H, $NCH_2CH_2CH_2$-Si), 1.15(*t*, J = 7.0 Hz, 9H, $NCH_2CH_2CH_2$-Si-$(OC_2H_5)_3$), 1.52(*m*, 2H, $NCH_2CH_2CH_2$-Si), 2.90(*m*, 8H, $N(CH_3)_2$, $NCH_2CH_2CH_2$-Si), 3.71(*q*, J = 7.0, 6H, $NHCH_2CH_2CH_2$-Si-$(OC_2H_5)_3$), 5.22(*s*, 1H, $NHCH_2CH_2CH_2Si$), 7.17(*d*, J = 7.2 Hz, 1H, CH_{DNS}), 7.52(*m*, 2H, CH_{DNS}), 8.24(*d*, J = 7.2 Hz, 1H, CH_{DNS}), 8.32(*d*, J = 8.4 Hz, 1H, CH_{DNS}), 8.52(*d*, J = 7.4 Hz, 1H, CH_{DNS}). ^{13}CNMR (100 MHz, $CDCl_3$, 25°C): δ (ppm) 7.32 ($NCH_2CH_2CH_2$-Si), 18.11 (NCH_2 -CH_2CH_2-Si-$(OCH_2CH_3)_3$), 22.92($NCH_2CH_2CH_2$-Si),45.29($N(CH_3)_2$),45.48(NCH_2-CH_2CH_2-Si), 58.31($NCH_2CH_2CH_2$-Si-$(OCH_2CH_3)_3$), 115.02, 118.74, 123.07, 128.16, 129.38, 129.55, 129.79, 130.15, 134.96, 151.86 (C_{DNS}).

DA/SBA-15 Composites: 100 mg of dried SBA-15 were suspended in 40 mL of anhydrous toluene in a round bottomed flask under nitrogen. The mixture was heated at 140°C to remove water by azeotropic distillation. After 30 mL of toluene was evaporated, the suspension was cooled to 90°C and 200 mg of DA-APTES was added. The mixture was stirred for 24 h at 115°C after supersonic treatment for 1 h. The modified SBA-15 were collected by filtration and repeatedly washed with anhydrous toluene, dichloromethane, and then ethanol under ultrasonic condition. Unreacted organic material was removed completely by monitoring the fluorescence of the washing liquid. After drying under vacuum, the desired product was obtained. The structure of the functional molecule and the SBA-15 modification procedure was showed in Scheme 1.

Instruments and Spectroscopic Measurements

Fourier transform infrared (FT-IR) spectra were recorded on a Nicolet NEXUS 670 FT-IR spectrometer (Nicolet, USA) by the standard KBr disk method. Low angle X-ray diffraction (XRD) analyses were performed on a Rigaku D/Max-2400 diffractometer (Rigaku, Japan), using Cu Kα radiation over the range of 0.5–6°. Transmission electron microscopy (TEM) measurements were taken on a Hitachi-600 electron microscope, with an accelerating voltage of

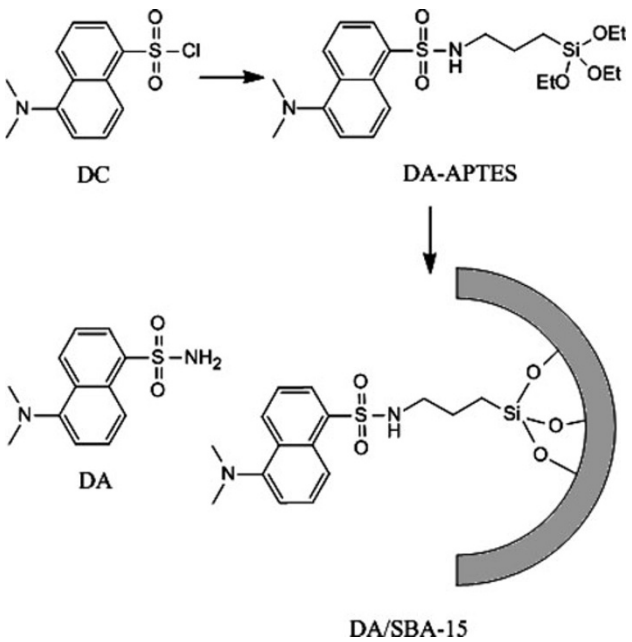

Scheme 1 The structure of the functional molecule and the SBA-15 modification procedure

100 kV. The thermogravimetric analysis (TGA) was carried out under N_2 atmosphere on Netzsch STA 449C equipment. The samples were heated at 10°C/min. Gmbh Varioel Elementar Analysensyteme was used to characterize the materials. The nitrogen adsorption/desorption experiments were performed at 77 K in a Micromeritics ASAP 2010 (USA). The samples were degassed at 373 K overnight before the measurement. Perkin Elmer LS 55 spectrofluorimeter was used to obtain the fluorescence spectra of the fluorescence material.

Results and Discussion

Figure 1 displays FTIR spectra of SBA-15 and DA/SBA-15 Composites, respectively. For SBA-15 and DA/SBA-15 Composites, the bands at 3,437 and 1,632 cm^{-1} are attributed to the stretching (3,437 cm^{-1}) and bending (1,632 cm^{-1}) vibrations of the surface silanol groups and the remaining adsorbed water molecules. In the two materials, the typical Si–O-Si bands around 1,080, 814 and 459 cm^{-1} associated with the formation of a condensed silica network are present. Additionally, the DA/SBA-15 system shows characteristic bands for aliphatic C–H stretching vibrations attributed to alkyl chains at around 3,000–2,800 cm^{-1}, N–H bending vibration around 692 cm^{-1} and -NH- deformation vibration at 1,509 cm^{-1}. The presence of DA-APTES in the modified SBA-15 was further corroborated by a broad band at 3,000–3,300 cm^{-1}, attributed to the NH stretching vibration.

The X-ray powder diffraction (XRD) patterns of SBA-15 and DA/SBA-15 are given in Fig. 2. Sample (a) is highly ordered, showing three strong diffraction peaks for the 100, 110 and 200 planes. Comparison of the diffraction patterns for sample (b) indicates that the 2D-hexagonal ordering has been retained after the binding of DA- APTES into mesopore channels of SBA-15. However, upon postsynthetic grafting, an overall attenuation in the intensity of the diffraction peaks was noticed. This attributed to the lowering of local order. Such a decrease in reflection intensity is interpreted as larger contrast in density between the silica walls and the open pores than that between the silica walls and the organic functional groups, which provides evidence that grafting occurs inside the mesopore channels. Complementary to the XRD data, the TEM images of the DA/SBA-15 exhibit highly ordered one-dimensional channels (Fig. 3b) compared with SBA-15 (Fig. 3a). It is clear that the hexagonal structure of SBA-15 was preserved after the functionalization.

The TGA curves of SBA-15 and DA/SBA-15 are shown in Fig. 4. According to curve a, there is a continuous weight lose of the SBA-15, and the amount of the weight lose is about 8.27% typical for raw SBA-15. From the TGA weight loss curve of DA/SBA-15 in Fig. 4, it can be seen that the content of the DA-APTES grafted to the SBA-15 is about 19.72 wt% comparing with curve a, which is similar to the calculation result of the elemental microanalysis (Table 1).

Nitrogen physisorption measurements of the DA/SBA-15 and the SBA-15 are shown in Fig. 5. The adsorption and desorption isotherms of both materials display type IV isotherms with H1-type hysteresis loops at the high relative pressure according to the IUPAC classification, which is a characteristic of capillary condensation within uniform pores. A sharp inflection in P/P_0 range from 0.6 to 0.8 is found both in isotherms of SBA-15 and DA/SBA-15, providing further proof on the maintaining of mesoporous structure after grafting [28, 29]. The texture parameters of

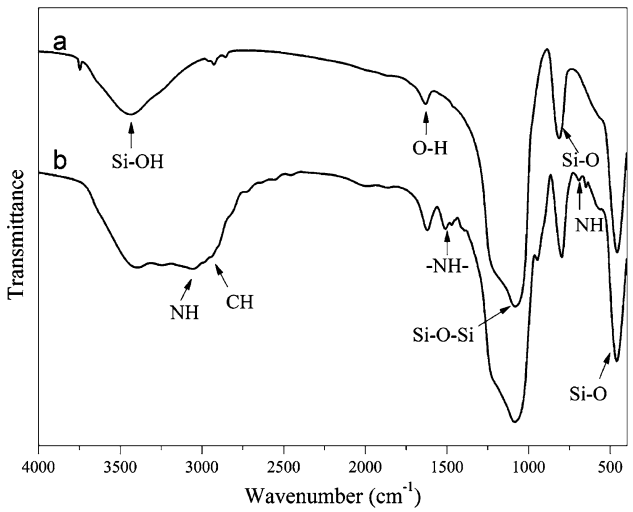

Fig. 1 FTIR spectra of a SBA-15 and b DA/SBA-15

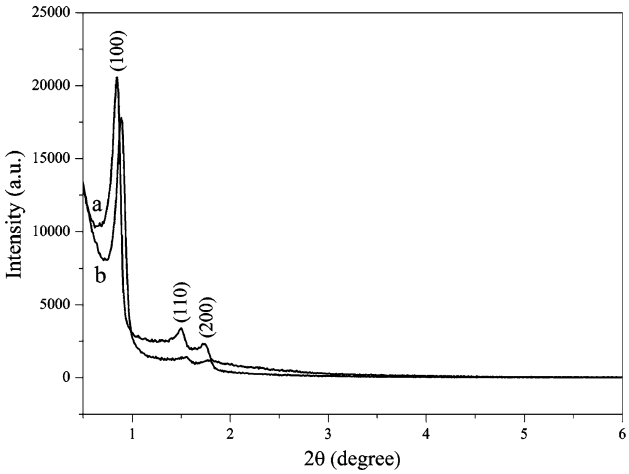

Fig. 2 Low-angle XRD patterns of **a** SBA-15 and **b** DA/SBA-15

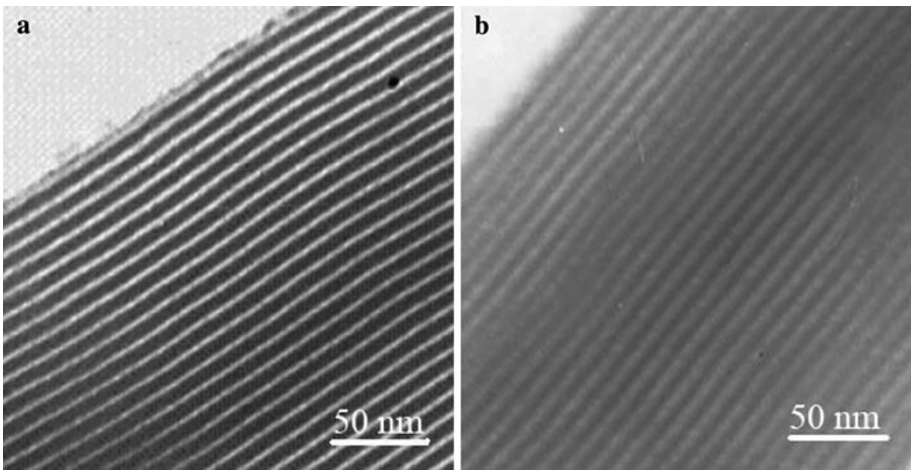

Fig. 3 TEM images of **a** SBA-15 and **b** DA/SBA-15

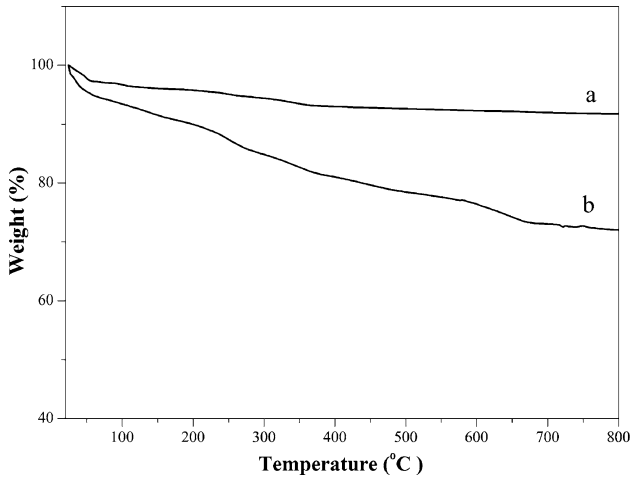

Fig. 4 TGA thermogram of **a** SBA-15 and **b** DA/SBA-15

Table 1 Elemental microanalysis for SBA-15 and DA/SBA-15

Element	Content (%) SBA-15	Content (%) 1
N	0.00	2.04
C	0.27	10.87
H	0.22	1.84

mesoporous silica SBA-15 were distinctly changed after grafting of DA-APTES. The functionalized hybrid materials exhibit a considerable decrease in BET surface area, pore volume and pore diameter. Our results indicate that the BET surface area is 667.21 m^2/g for SBA-15, but decreases to 290.14 m^2/g for the hybrid material, and correspondingly, the pore volume shrinks to 0.59 cm^3/g from 1.06 cm^3/g for the parent material. Pore size distributions presented as BJH plots are inserted in Fig. 5. As can be seen, the BJH pore diameters distribution for the resultant is relatively narrow with a maximum at 5.03 nm, which shows a decrease in diameter by 1.06 nm compared with that of parent SBA-15. The decrease in BET surface area, pore volume and diameters gives additional proof of the grafting of the fluorescent chromophore onto the surface of the inner channel.

Figure 6 compares the fluorescence spectra of DA-APTES before and after being anchored into SBA-15. The emission band (excitation 335 nm) of DA-APTES appears at 527 nm (curve b in Fig. 6), whereas a typical emission band (excitation 335 nm) emerges at 500 nm in the spectrum of DA/SBA-15 (curve a in Fig. 6), which characterizes a significant blue shift after the DA-APTES molecules are anchored in the channel of SBA-15. Zhang et al. [30] interpreted this phenomenon by the molecular orbital confinement theory that all energy levels of guest molecules increase in the channel of the host as a result of the confinement. Consequently, the reason of the blue shift in our experiments may be the same as that reported by Zhang et al. In our hybrid complex, the increase in the energy

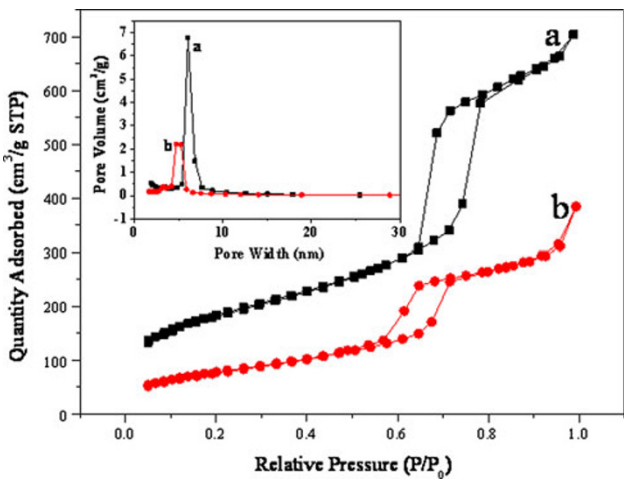

Fig. 5 N_2 adsorption–desorption isotherms of **a** SBA-15 and **b** DA/SBA-15. The insert corresponding pore size distribution for **a** SBA-15 and **b** DA/SBA-15

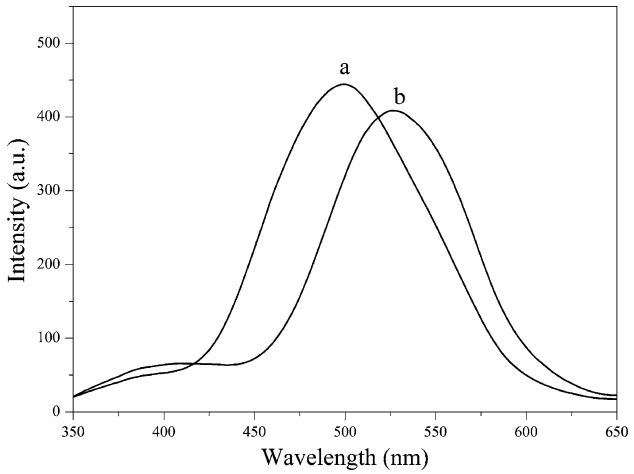

Fig. 6 Fluorescence spectrum of **a** DA-APTES (1×10^{-5} M) and **b** DA/SBA-15 (1×10^{-5} M) in 15% ethanol/water solution. λex = 335 nm

level of the DA-APTES molecule probably results in the blue shift on the spectrum of DA/SBA-15.

The sensitivity of fluorescence quenching from DA/SBA-15 by Hg^{2+} was also investigated, and the results are described in Fig. 7a. The fluorescence intensity of DA/SBA-15 gradually decreased with increasing Hg^{2+} concentration. And finally when the concentration of Hg^{2+} reached to 1×10^{-3} M, the fluorescence intensity quenched to 29%. The detection limit for Hg^{2+} is established at 10^{-6} M under current experimental conditions (Fig. 7b). The result of a titration of DA/SBA-15 with Hg^{2+} ions is shown in Fig. 7. Addition of 15 equivalents of Hg^{2+} ions caused 57% quenching of fluorescence of DA/SBA-15.

Many different optical applications use DA as fluorophore when it is linked to a receptor [31–34]. Mu et al. [35] reported a covalent immobilization of DA on SiNWs to form DA-SiNWs by the synthesis of 3-(dansylamino)propyltriethoxysilane and that the fluorescence of DA-SiNWs exhibited selective responses to Hg^{2+} ions. The experimental results suggest that the dependence of the fluorescence intensity of DA in the presence of various ions is similar to that of DA-SiNWs. Hg^{2+} ions effectively quench the fluorescence of DA, whereas other metal ions cause a negligible fluorescence change. The fact that Pb^{2+} ions do not quench the fluorescence of DA suggest that the quenching action of Hg^{2+} ions is unlikely to be associated with the heavy atom effect. Rather, the fluorescence quenching may be attribute to charge transfer within DA and Hg^{2+} ions [31, 32]. In our experiment, the minimum ratio of Hg^{2+} ions to DA/SBA-15 to achieve maximum quenching from the titration data between Hg^{2+} ions and DA/SBA-15 was 12. In order to assure maximum

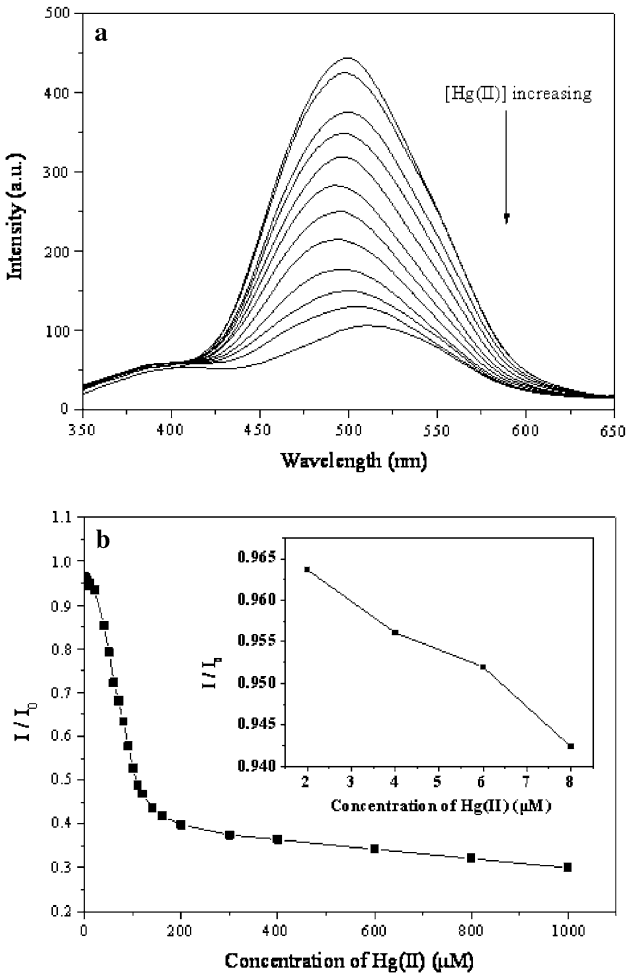

Fig. 7 **a** Fluorescence spectra of DA/SBA-15 with Hg^{2+}, **b** Relative fluorescence intensity of DA/SBA-15 at different concentration of Hg^{2+}. DA/SBA-15 (1×10^{-5} M) in 15% ethanol/water solution. λex = 335 nm

quenching, we take 1:15 stoichiometry to detect the selectivity of DA/SBA-15.

According to 1:15 stoichiometry, a series of experiment has been done to determine the selectivity of DA/SBA-15. The inorganic–organic hybrid chemosensor was well dispersed in a mixture solvent of 15% ethanol/water because of the solvent's strong polarity. Figure 8 depicts the plots of I/I_0 against the titration of various metal ions in the presence of DA/SBA-15 in 15% ethanol/water solution at pH 7.0, where I_0 and I stand for the fluorescence intensity of the material analyzed at 335 nm in the absence and presence of metal ions. The fluorescence properties of DA/SBA-15 in the presence of different metal ions are shown in Fig. 8, which indicates that only Hg^{2+} ions quench the fluorescence of DA/SBA-15. No noticeable fluorescence changes of DA/SBA-15 were observed on addition of other metal ions M (M = Zn^{2+}, Cd^{2+}, Fe^{2+}, Co^{2+}, Ni^{2+}, Pb^{2+}, Cu^{2+}, Ag^{+}, K^{+}, Ca^{2+},

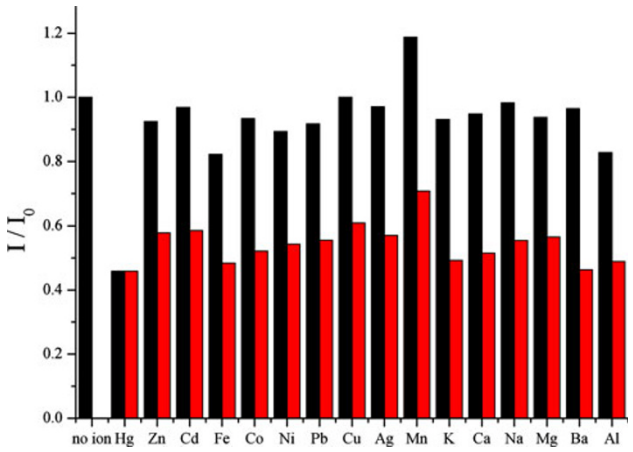

Fig. 8 Relative fluorescence intensity of DA/SBA-15 (1×10^{-5} M) in the presence of various interfering ions (0.15 mM, *black bars*) and coexistence (*red bars*) of interfering ions (0.15 mM) with Hg^{2+} (0.15 mM), in 15% ethanol/water solution (λex = 335 nm). Interfering ions containing *1* no ions, *2* Hg^{2+}, *3* Zn^{2+}, *4* Cd^{2+}, *5* Fe^{2+}, *6* Co^{2+}, *7* Ni^{2+}, *8* Pb^{2+}, *9* Cu^{2+}, *10* Ag^{+}, *11* Mn^{2+}, *12* K^{+}, *13* Ca^{2+}, *14* Na^{+}, *15* Mg^{2+}, *16* Ba^{2+}, *17* Al^{3+}

Na^{+}, Mg^{2+}, Ba^{2+}, Al^{3+}). Only Mn^{2+} induces a slight enhancement of the fluorescence of DA/SBA-15, which may be due to the coordinate effect. As a result, the DA/SBA-15 shows a high selectivity to Hg^{2+} ions.

Conclusion

We have prepared a new inorganic–organic hybrid sensing material based on SBA-15 as support and DA as fluorescent center. The results of the fluorescence characterization showed that the composite has a highly selective and sensitive (10^{-6}M) detection for Hg^{2+} and revealed that ratiometric Hg^{2+} sensing is possible with fluorophore chemically modified SBA-15. This novel fluorescent material may be used as a fluorescent device in aqueous solution for the detection of Hg^{2+}.

References

1. L. Xue, C. Liu, H. Jiang, Chem. Commun. **9**, 1061 (2009)
2. Q. Miao, X.B. Huang, Y.Q. Cheng, Y. Liu, L.L. Zong, Y.X. Cheng, J. Appl. Polym. Sci. **111**, 3137 (2009)
3. V.B. Bojinov, I.P. Panova, Dyes Pigments **80**, 61 (2009)
4. R. Martínez, A. Espinosa, A. Tárraga, P. Molina, Tetrahedron **64**, 2184 (2008)
5. M. Arduini, L. Armelao, S. Gross, F. Mancin, S. Marcuz, M. Montolli, C. Sada, Appl. Surf. Sci. **253**, 7178 (2007)
6. G. Farruggia, S. Iotti, L. Prodi, M. Montalti, N. Zaccheroni, P.B. Savage, V. Trapani, P. Sale, F.I. Wolf, J. Am. Chem. Soc. **128**, 344 (2006)
7. S. Yoon, E.W. Miller, Q. He, P.H. Do, C.J. Chang, Angew. Chem. Int. Ed. **46**, 6658 (2007)
8. S. Yoon, A.E. Albers, A.P. Wong, C.J. Chang, J. Am. Chem. Soc. **127**, 16030 (2005)
9. H. Yang, Z. Zhou, K. Huang, M. Yu, F. Li, T. Yi, C. Huang, Org. Lett. **9**, 4729 (2007)
10. A. Renzoni, F. Zino, E. Franchi, Environ. Res. **77**, 68 (1998)
11. B.O. Stephan, L. Beate, R.M. Gothe, C. Beinhoff, U. Siebert, G. Drasch, Environ. Res. **107**, 89 (2008)
12. D. Naftz, C. Angeroth, T. Kenney, B. Waddell, N. Darnall, S. Silva, C. Perschon, J. Whitehead, Appl. Geochem. **23**, 1731 (2008)
13. H.S. Zhou, H. Sasabe, I. Honma, J. Mater. Chem. **8**, 515 (1998)
14. A. Stein, B.J. Melde, R.C. Schroden, Adv. Mater. **12**, 1403 (2000)
15. M. Boiocchi, M. Bonizzoni, L. Fabbrizzi, G. Piovani, A. Taglietti, Angew. Chem. Int. Ed. **43**, 3847 (2004)
16. M. Comes, G.R. Lopez, M.D. Marcos, R.M. Manez, F. Sancenon, J. Soto, L.A. Villaescusa, P. Amoros, D. Beltran, Angew. Chem. Int. Ed. **44**, 2918 (2005)
17. J.L. Shi, Z.L. Hua, L.X. Zhang, J. Mater. Chem. **14**, 795 (2004)
18. R.J.P. Corriu, A. Mehdi, C. Reyé, C. Thieuleux, Chem. Commun. **13**, 1382 (2002)
19. O. Olkhovyk, M. Jaroniec, J. Am. Chem. Soc. **127**, 60 (2005)
20. R.J.P. Corriu, E. Lancelle-Beltran, A. Mehdi, C. Reyé, S. Brandès, R. Guilard, Chem. Mater. **15**, 3152 (2003)
21. V.S.Y. Lin, C.Y. Lai, J. Huang, S.A. Song, S. Xu, J. Am. Chem. Soc. **123**, 11510 (2001)
22. A.B. Descalzo, K. Rurack, H. Weisshoff, R. Manez, M. Dolores, P. Amoros, K. Hoffmann, J. Sato, J. Am. Chem. Soc. **127**, 184 (2005)
23. W. Xu, D.L. Akins, J. Phys. Chem. B **106**, 1991 (2002)
24. C. Bargossi, M.C. Fiorini, M. Montalti, L. Prodi, F. Bolletta, N. Zaccheroni, Coord. Chem. Rev. **208**, 17 (2000)
25. C.F. Chen, Q.Y. Chen, Tetrahedron Lett. **45**, 3957 (2004)
26. D. Zhao, J. Feng, Q. Huo, N. Melosh, G.H. Fredrickson, B.F. Chmelka, G.D. Stucky, Science **279**, 548 (1998)
27. M. Arduini, S. Marcuz, M. Montolli, E. Rampazzo, F. Mancin, S. Gross, L. Armelao, P. Tecilla, U. Tonellato. Langmuir **21**, 9314 (2005)
28. J.Q. Wang, L. Huang, M. Xue, Y. Wang, L. Gao, J.H. Zhu, Z. Zou, J. Phys. Chem. C **112**, 5014 (2008)
29. F. Zhang, Y. Yan, H. Yang, Y. Meng, C. Yu, B. Tu, D. Zhao, J. Phys.Chem. B **109**, 8723 (2005)
30. L. Zhang, Y. Xiong, P. Cheng, G. Tang, D. Zheng, Chem. Phys. Lett. **358**, 278 (2002)
31. R. Métivier, I. Leray, B. Valeur, Chem. Eur. J. **10**, 4480 (2004)
32. R. Métivier, I. Leray, B. Lebeau, B. Valeur, J. Mater. Chem. **15**, 2965 (2005)
33. Q.Y. Chen, C.F. Chen, Tetrahedron Lett. **46**, 165 (2005)
34. Y. Zhao, Z. Zhong, Org. Lett. **8**, 4715 (2006)
35. L. Mu, W. Shi, G. She, J.C. Chang, S.T. Lee, Angew. Chem. Int. Ed. **48**, 3469 (2009)